

Analysis of high-speed vehicle-bridge interactions by a simplified 3-D model

Myung-Kwan Song[†] and Chang-Koon Choi[‡]

*Department of Civil and Environmental Engineering, Korea Advanced Institute of
Science and Technology, Daejeon 305-701, Republic of Korea*

(Received October 19, 2001, Accepted March 23, 2002)

Abstract. In this study, the analysis of high-speed vehicle-bridge interactions by a simplified 3-dimensional finite element model is performed. Since railroads are constructed mostly as double tracks, there exists eccentricity between the vehicle axle and the neutral axis of cross section of a railway bridge. Therefore, for the more efficient and accurate vehicle-bridge interaction analysis, the analysis model should include the eccentricity of axle loads and the effect of torsional forces acting on the bridge. The investigation into the influences of eccentricity of the vehicle axle loads and vehicle speed on vehicle-bridge interactions are carried out for two cases. In the first case, only one train moves on its track and in the other case, two trains move respectively on their tracks in the opposite direction. From the analysis results of an existing bridge, the efficiency and capability of the simplified 3-dimensional model for practical application can be also verified.

Keywords: railway bridge; vehicle-bridge interaction analysis; double tracks; eccentricity of vehicle axle loads; influence of eccentricity; influence of vehicle speed.

1. Introduction

Willis (1849), Timoshenko (1920's), and Inglis (1930's) are the earlier contributors to the technical advancement in the impact and vibration problem of railway bridges. However, their studies were based on the simple models, which were intended to represent a steam locomotive moving on a bridge. Also, a number of experimental studies on railway bridge vibrations were carried out by Robinson (1887) and Hunley (1936) and the extensive tests of impact on railway bridges were reported by a subcommittee of the American Railway Engineering Association (AREA) (Turneaure 1911 and Ruble 1955). A realistic attempt to systematically analyze the dynamic responses of a girder and a truss bridge during the passage of a series of railway vehicles was made by Dhar (1978). In his study, both the bridge and vehicles were assumed to have vertical motions only. Wiriyachi (1980) investigated into the effects of the impact on an open-deck truss bridge and developed 3-dimensional bridge models to study fatigue failures of critical members.

Wiriyachi's work has been followed by many other researches. However, in most of these researches, only the vertical interaction between the bridge and vehicles has been considered, using

[†] Ph.D. Student

[‡] Institute Chair Professor

the simplified vehicle models which do not take into account many important geometric and suspension nonlinearities present in an actual freight car. In addition, because of the limitations in the formulation of vehicle-bridge interaction models, the effect of vehicle motion prior to the entry onto the bridge has been accounted for by simply assigning certain initial displacement and/or rolling motion values to all the vehicles in the train. Bhatti (1982) proposed the 3-dimensional vehicle-bridge interaction model which took into consideration the significant geometric and suspension nonlinearities present in an actual freight car. The dynamic responses and impact factors of various members of an open-deck bridge were determined by including both vertical and lateral interactions between the bridge and vehicle, and the vertical and lateral track irregularities. Hino (1985) and Chang (1996) proposed a finite element analysis for the vibration of bridges loaded by moving vehicles considering geometric nonlinearities of bridges.

Recently, to increase the operating speed of trains has received a lot of researchers' attention in many countries. As for the commercial operating speed, TGV (le train de grande vitesse, France) and Shinkansen (Japan) are being operated at about 300 km/h, ICE (Germany) is being operated at 280 km/h, and KTX (Korea Train eXpress; Korea-version TGV) is due to be operated at 300 km/h in Korea. As the speed of trains becomes higher and the operating speed of train reaches 300 km per hour or more, the more accurate analysis of vehicle-bridge interactions becomes the more important factor to be considered for bridge design. Using the 2-dimensional model for vehicle-bridge interactions, the analysis for the effect of some parameters, i.e., characteristics of stiffness and mass of the bridge, stiffness of the train, bridge span, and track irregularities, was performed by Delgado (1997). Yang (1994) proposed the dynamic condensation method for vehicle-bridge interaction analysis. Yang (1997) also investigated the key parameters that govern the dynamic responses of the simple beams by an analytical approach using moving load assumption. Tanabe (1997) developed a 3-dimensional analysis program for the dynamic interaction analysis for Shinkansen trains and railway bridges. Fafard (1996) proposed also a 3-dimensional analysis model to study the vehicle-bridge interactions, in which the bridge was modeled with plate and beam finite elements and the vehicle was modeled with 5 axles. Mermerta (1997) analyzed the interaction between the vehicle and the simply supported curved bridge deck. Tan (1998) introduced the grillage analysis method for the vehicle-bridge interactions to consider the nonlinear behavior of suspension in an actual vehicle and the yield surface of materials of bridges. Recently, Li (1999) studied the dynamic responses of a simply supported girder bridge under high-speed trains with the emphasis on the resonant vibration using moving load analysis and vehicle-bridge interaction analysis. Yang (2001) derived a versatile element that was capable of treating various vehicle-bridge interaction effects. In most of the previous 2-dimensional analysis models, the influence of the eccentricity between the axle loads of vehicles and the neutral axis of cross section of the bridge cannot be considered, whereas the full 3-dimensional analysis models require a lot of modeling and computing efforts.

In this study, the analysis of high-speed vehicle-bridge interactions by a simplified 3-dimensional finite element model is performed. This simplified 3-dimensional analysis model can improve the accuracy of 2-dimensional analysis nearly to the level of full 3-dimensional analysis and reduce modeling and computing efforts as well. This study focuses on the analytical formulations of motion of the total vehicle-bridge system and on the applications of the proposed method to numerical examples. The calculation of vertical deflections and torsional rotations are emphasized as the member forces (bending moments, torsional moments, and shear forces) of bridge elements are easily obtained based on the deflections. In addition, an intensive investigation into the influences of the eccentricity of axle loads and the vehicle speed on vehicle-bridge interactions are carried out for

two cases. In the first case, only one train moves on the one side of a bridge and in the other case, two trains move respectively on their tracks in the opposite direction.

2. Vehicle model

Lagrange's equations for the vehicle-bridge system are derived based on the model shown in Fig. 1. In the ordinary train vehicles, there are two bogies in the fore and rear parts of the car body and thus the adjacent car bodies move separately and as a result, the relatively large vibration in each car body may be generated. In this study, bogies are connected at the joints between car bodies so that a series of car bodies move on the track just like one organic body. Thus, the vibration

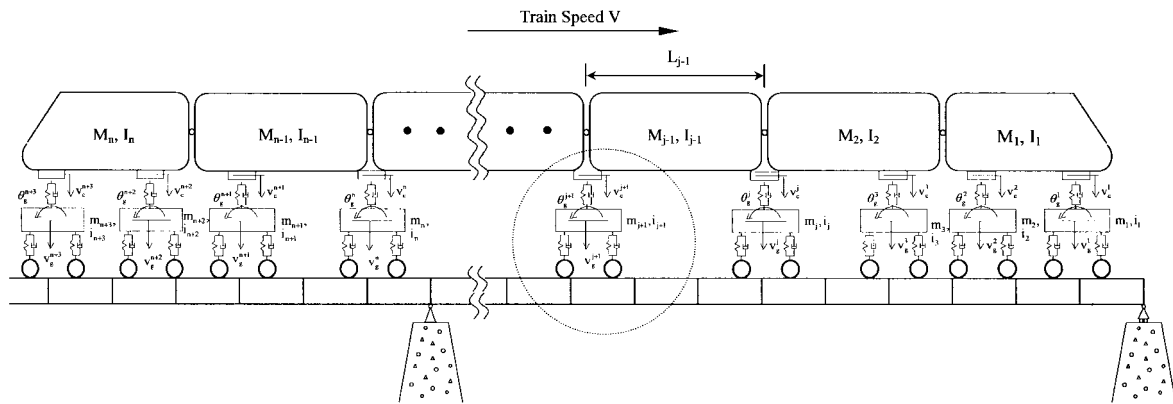


Fig. 1 A model for high-speed vehicle-bridge interaction analysis

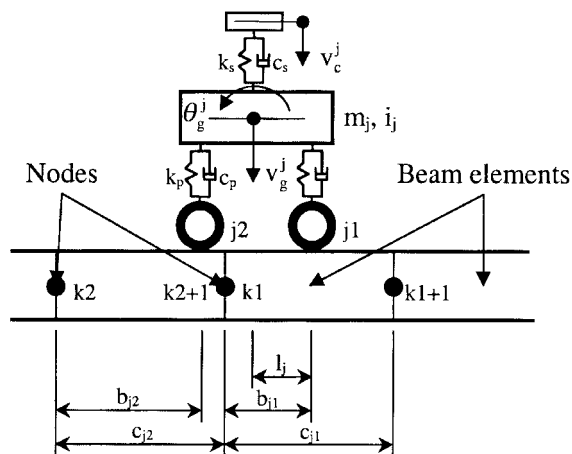


Fig. 2 The relation between the positions of axles and the nodes of beam elements

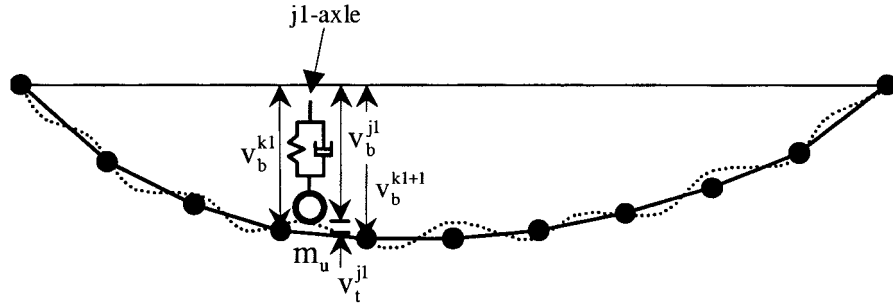


Fig. 3 The relation between motion of unsprung mass and vertical deflections of nodes

generated in each car body, in particular at the connections of two car bodies, can be reduced to the considerably low level. The combined effect of bouncing and pitching motions of car bodies and bogies generates the vertical and rotational degrees of freedom (d.o.f.) in the bogie and joint between car bodies. As shown in Fig. 2, the bouncing and pitching motions of car bodies are expressed by the vertical d.o.f. (v_c) at the joints of bogies. And, the bouncing and pitching motions of bogies are expressed by the vertical (v_g) and rotational d.o.f. (θ_g) at the center of bogies, respectively. For the simplicity, it is assumed that car bodies and bogies are rigid bodies with masses and that they move along a straight track with constant speed.

For the Lagrange's equations of motion, the kinetic energy, potential energy, and damping energy of power cars and passenger cars are expressed by the vertical and rotational degrees of freedom at joints, bogies, and a bridge.

2.1 Power cars

The kinetic energy, potential energy, and damping energy of the entire vehicles are separately expressed in two categories; power cars and passenger cars. For many vehicles, for example, the motive power for KTX is supplied by the front and rear power cars. A series of passenger cars are connected in a line between these two power cars and motor coach motor bogies are set up in the fore and rear part of the each power car.

The kinetic energy of power cars (E_k) is expressed by the degrees of freedom of bogies and joints of power cars as in Eqs. (1) and (2)

For a front power car :

$$E_k = \left\{ \frac{1}{2} M_1 \left(\frac{\dot{v}_c^1 + \dot{v}_c^2}{2} \right)^2 + \frac{1}{2} I_1 \left(\frac{\dot{v}_c^1 - \dot{v}_c^2}{L_1} \right)^2 \right\} + \sum_{j=1}^2 \frac{1}{2} m_j \dot{v}_g^{j^2} + \sum_{j=1}^2 \frac{1}{2} i_j \dot{\theta}_g^{j^2} \quad (1)$$

For a rear power car :

$$E_k = \left\{ \frac{1}{2} M_n \left(\frac{\dot{v}_c^{n+2} + \dot{v}_c^{n+3}}{2} \right)^2 + \frac{1}{2} I_n \left(\frac{\dot{v}_c^{n+2} - \dot{v}_c^{n+3}}{L_n} \right)^2 \right\} + \sum_{j=n+2}^{n+3} \frac{1}{2} m_j \dot{v}_g^{j^2} + \sum_{j=n+2}^{n+3} \frac{1}{2} i_j \dot{\theta}_g^{j^2} \quad (2)$$

where M_k = mass of k -th car body, I_k = moment of inertia for pitching of k -th car body, L_k = length of k -th car body, m_j = mass of j -th bogie, i_j = moment of inertia for pitching of j -th bogie, v_c^j = vertical d.o.f. in the joint connected with j -th bogie between two car bodies, v_g^j = vertical d.o.f. in the center of j -th bogie, θ_g^j = rotational d.o.f. in the center of j -th bogie, and n = total number of car bodies as shown in Figs. 1 and 2, and a dot (\cdot) represents the time derivative.

The potential energy (E_p) is defined by the primary and secondary suspension springs set up in bogies and joints. It can be expressed by the degrees of freedom of joints, bogies, and bridges as in Eqs. (3) and (4).

For a front power car :

$$E_p = \sum_{j=1}^2 \frac{1}{2} k_s (v_c^j - v_g^j)^2 + \sum_{j=1}^2 \frac{1}{2} k_p v_r^{j1^2} + \sum_{j=1}^2 \frac{1}{2} k_p v_r^{j2^2} \quad (3)$$

For a rear power car :

$$E_p = \sum_{j=n+2}^{n+3} \frac{1}{2} k_s (v_c^j - v_g^j)^2 + \sum_{j=n+2}^{n+3} \frac{1}{2} k_p v_r^{j1^2} + \sum_{j=n+2}^{n+3} \frac{1}{2} k_p v_r^{j2^2} \quad (4)$$

where k_p = spring constant of the primary suspension, k_s = spring constant of the secondary suspension, and v_r^{jl} = relative vertical deformation of the primary suspension at the l -th wheel-rail contact point ($l = 1, 2$) of j -th bogie.

The damping energy (E_d) is defined by the primary and secondary suspension dampers set up in bogies and joints. It can be expressed by the degrees of freedom of joints, bogies, and a bridge as in Eqs. (5) and (6).

For a front power car :

$$E_d = \sum_{j=1}^2 \frac{1}{2} c_s (\dot{v}_c^j - \dot{v}_g^j)^2 + \sum_{j=1}^2 \frac{1}{2} c_p \dot{v}_r^{j1^2} + \sum_{j=1}^2 \frac{1}{2} c_p \dot{v}_r^{j2^2} \quad (5)$$

For a rear power car :

$$E_d = \sum_{j=n+2}^{n+3} \frac{1}{2} c_s (\dot{v}_c^j - \dot{v}_g^j)^2 + \sum_{j=n+2}^{n+3} \frac{1}{2} c_p \dot{v}_r^{j1^2} + \sum_{j=n+2}^{n+3} \frac{1}{2} c_p \dot{v}_r^{j2^2} \quad (6)$$

where c_p = damping coefficient of the primary suspension and c_s = damping coefficient of the secondary suspension.

2.2 Passenger cars

The kinetic energy, potential energy, and damping energy of passenger cars can be obtained in the similar manner as mentioned in the previous section. Intermediate carrying bogies are set up in the front and back end of respective passenger car, while trailer motor bogies are set up between power cars and passenger cars. The kinetic energy, potential energy, and damping energy of passenger cars

are expressed in the following equations.

$$E_k = \sum_{j=3}^n \left\{ \frac{1}{2} M_{j-1} \left(\frac{\dot{v}_c^j + \dot{v}_c^{j+1}}{2} \right)^2 + \frac{1}{2} I_{j-1} \left(\frac{\dot{v}_c^j - \dot{v}_c^{j+1}}{L_{j-1}} \right)^2 \right\} + \sum_{j=3}^{n+1} \frac{1}{2} m_j \dot{v}_g^{j^2} + \sum_{j=3}^{n+1} \frac{1}{2} i_j \dot{\theta}_g^{j^2} \quad (7)$$

The potential energy is defined by the primary and secondary suspension springs set up in bogies and joints.

$$E_p = \sum_{j=3}^{n+1} \frac{1}{2} k_s (v_c^j - v_g^j)^2 + \sum_{j=3}^{n+1} \frac{1}{2} k_p v_r^{j1^2} + \sum_{j=3}^{n+1} \frac{1}{2} k_p v_r^{j2^2} \quad (8)$$

The damping energy is defined by the primary and secondary suspension dampers set up in bogies and joints.

$$E_d = \sum_{j=3}^{n+1} \frac{1}{2} c_s (\dot{v}_c^j - \dot{v}_g^j)^2 + \sum_{j=3}^{n+1} \frac{1}{2} c_p \dot{v}_r^{j1^2} + \sum_{j=3}^{n+1} \frac{1}{2} c_p \dot{v}_r^{j2^2} \quad (9)$$

3. Bridge model

3.1 Modeling of a bridge

A simple but reasonably accurate 3-D model for the bridge that the influence of eccentricity of axle loads can be considered may be the use of the beam finite element in which the torsional rotation (ϕ_b) is included in addition to 2 degrees of freedom at each node, i.e., the vertical deflection (v_b) and rotation (θ_b), as shown in Fig. 4. In the present study, the bridge with variable cross-section is approximately modeled by beam elements with segment-wise constant cross sections. At supports, the vertical deflections (v_b) and torsional rotations (ϕ_b) are restrained but the rotations (θ_b) are free. The vertical deformations occurred in the piers and torsional rotations produced at supports due to the train loading are not considered because they are negligibly small. Therefore, the current study is focused on the behavior of the superstructure of a bridge. The bridge in this study is assumed to be straight and the formulation of element stiffness and mass matrices can be found in many



Fig. 4 Degrees of freedom of beam element

published literatures (Przemieniecki 1968).

3.2 Track irregularities

In this study, only the vertical roughness of rail (or track irregularities) is considered in the interactions between vehicles (wheels) and rails. To define the track irregularities along the distance, the power spectral density (PSD) function needs to be assumed and then the generation of random number and inverse Fourier transform are needed.

Track irregularities are considered as stationary and ergodic processes in the space, i.e., random functions in the longitudinal coordinate x , and are characterized most frequently by PSD function, $S_z(\gamma)$. The PSD function depends on the wave number (γ) which is expressed as in Eq. (10).

$$\gamma = \frac{1}{\lambda} = \frac{1}{VT} = \frac{\omega}{2\pi} \quad (10)$$

where λ is the wave length, T is the period of wave, V is the vehicle speed, and ω is the circular frequency of wave.

The PSD functions for the generation of track irregularities have been proposed by many organizations and institutes for the applications in practice such as SNCF of France, FRA of USA and CSD, ZZO, SZD of Czech Republic. Thus, the different PSD functions are used depending on the characteristics of rails used in each country. In the present study, the formula in Eq. (11), which is similar to the PSD function proposed by the practical measurement of French National Railways (SNCF), is used.

$$S_z(\gamma) = \frac{A}{(B + \gamma)^3} \quad (\text{m}^3) \quad (11)$$

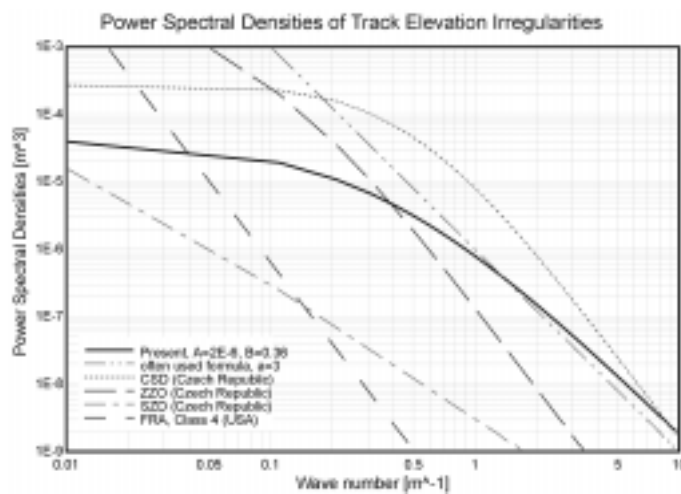


Fig. 5 PSD functions for the generation of track irregularities

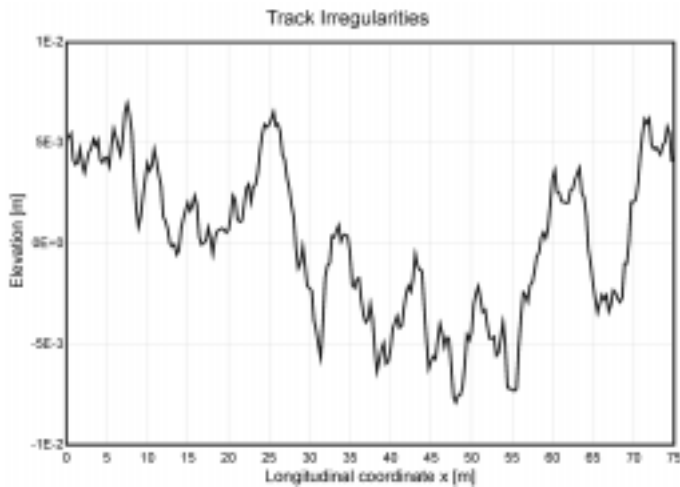


Fig. 6 Track irregularities as longitudinal coordinate x

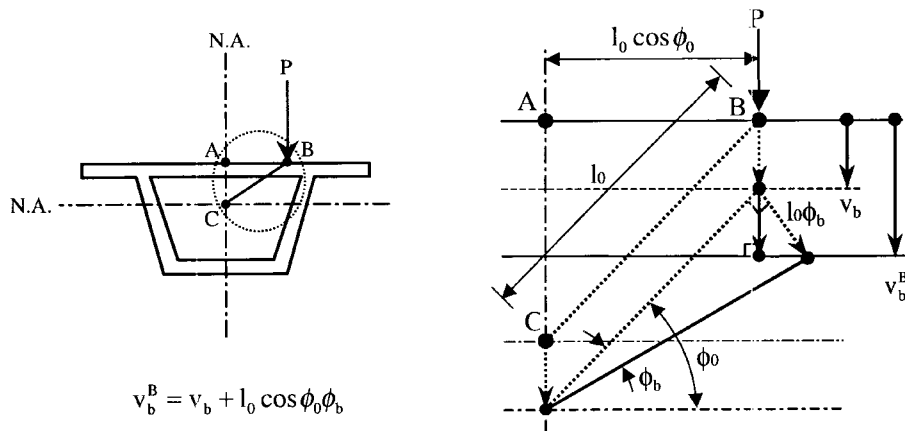


Fig. 7 Modeling of the eccentricity of axle loads

where $A = 2.0 \times 10^{-6}$, $B = 0.36$ are used. By using 1024 spectra, the vertical track irregularities are generated with respect to the longitudinal coordinate x as shown in Fig. 6. The coefficients of A and B in Eq. (11) are the values related to track irregularities (roughness). A is a constant for the short waves whose wave lengths are shorter than 3 m and B is a constant for the long waves longer than 3 m.

3.3 Modeling of the eccentricity of axle loads

In the 2-dimensional vehicle-bridge interaction analysis, it is assumed that the axle loads of vehicles are applied on the neutral axis of cross-section of the bridge. However, since railroads are constructed mostly as double tracks, the eccentricity between the axles and the neutral axis of the cross-section of the bridge should be considered in the analysis of railway bridges.

When an axle load P is applied at the position apart from the neutral axis of cross-section by a distance $\overline{AB}(=l_0 \cos \phi_0)$, the vertical deflection (v_b) and torsional rotation (ϕ_b) in the neutral axis of cross section of the bridge are produced simultaneously as seen in Fig. 7. Thus, the vertical deflection of $l_0 \cos \phi_0 \phi_b$, which is additional to the vertical deflection (v_b) in the neutral axis of cross-section at the position of axle, is generated and the vertical deflection (v_b^B) at the position of axle, i.e., point B in Fig. 7, becomes $v_b + l_0 \cos \phi_0 \phi_b$. Hence, when vehicles move on the track with the eccentricity of \overline{AB} , the relative vertical deformations of the primary suspensions at the wheel-rail contact points are extended by $l_0 \cos \phi_0 \phi_b$.

The vertical deformations of the primary suspensions at the wheel-rail contact points of two vehicle axles of j -th bogie, as shown in Eqs. (3)-(6), (8), and (9), are defined as Eqs. (12) and (13) considering the torsional rotation of the bridge generated by the eccentricity of vehicle axle.

$$v_r^{j1}(x, t) = v_g^j(x, t) - l_j \theta_g^j(x, t) - \{v_b^{j1}(x, t) - v_t^{j1}(x, t)\} - l_0 \cos \phi_0 \phi_b^{j1}(x, t) \quad (12)$$

$$v_r^{j2}(x, t) = v_g^j(x, t) + l_j \theta_g^j(x, t) - \{v_b^{j2}(x, t) - v_t^{j2}(x, t)\} - l_0 \cos \phi_0 \phi_b^{j2}(x, t) \quad (13)$$

In Eqs. (12) and (13), v_t^{j1} and v_t^{j2} are the elevations of the first and second axle of j -th bogie due to the track irregularities, respectively. Similarly, v_b^{j1} and v_b^{j2} are the vertical deflections and ϕ_b^{j1} and ϕ_b^{j2} are the torsional rotations under the two vehicle axles of j -th bogie on the bridge. Also, the vertical deflection under vehicle axle is interpolated from vertical deflections at the nodes of the bridge model as given in the following equations and as also shown in Figs. 2 and 3.

$$v_b^{j1} = \beta_{j1} v_b^{k1} + \alpha_{j1} v_b^{k1+1} \quad (14)$$

$$v_b^{j2} = \beta_{j2} v_b^{k2} + \alpha_{j2} v_b^{k2+1} \quad (15)$$

$$\phi_b^{j1} = \beta_{j1} \phi_b^{k1} + \alpha_{j1} \phi_b^{k1+1} \quad (16)$$

$$\phi_b^{j2} = \beta_{j2} \phi_b^{k2} + \alpha_{j2} \phi_b^{k2+1} \quad (17)$$

where $\alpha_{j1} = b_{j1}/c_{j1}$, $\beta_{j1} = 1 - \alpha_{j1}$, $\alpha_{j2} = b_{j2}/c_{j2}$, and $\beta_{j2} = 1 - \alpha_{j2}$.

Therefore, by substituting Eqs. (14)-(16), and (17) into Eqs. (12) and (13), the vertical deformations of the primary suspensions at the wheel-rail contact points of two vehicle axles of j -th bogie are obtained by the following equations.

$$\begin{aligned} v_r^{j1}(x, t) &= v_g^j(x, t) - l_j \theta_g^j(x, t) - \{\beta_{j1} v_b^{k1} + \alpha_{j1} v_b^{k1+1} - v_t^{j1}(x, t)\} \\ &\quad - (\beta_{j1} l_0 \cos \phi_0 \phi_b^{k1} + \alpha_{j1} l_0 \cos \phi_0 \phi_b^{k1+1}) \end{aligned} \quad (18)$$

$$\begin{aligned} v_r^{j2}(x, t) &= v_g^j(x, t) + l_j \theta_g^j(x, t) - \{\beta_{j2} v_b^{k2} + \alpha_{j2} v_b^{k2+1} - v_t^{j2}(x, t)\} \\ &\quad - (\beta_{j2} l_0 \cos \phi_0 \phi_b^{k2} + \alpha_{j2} l_0 \cos \phi_0 \phi_b^{k2+1}) \end{aligned} \quad (19)$$

And by substituting Eqs. (18) and (19) into Eqs. (3)-(6), (8), and (9), the equations for the kinetic energy, potential energy, and damping energy of the vehicle-bridge system can be expressed by the degrees of freedom of joints, bogies, and a bridge.

4. Equations of motion of vehicle-bridge system

The equations of motion for the problem can be derived by substituting equations which define the kinetic energy, potential energy, and damping energy of power cars and passenger cars (Eqs. (1)-(9)) into the Lagrange's equations.

$$\frac{d}{dt} \left(\frac{\partial E_k}{\partial \dot{q}_t} \right) - \frac{\partial E_k}{\partial q_t} + \frac{\partial E_p}{\partial q_t} + \frac{\partial E_d}{\partial \dot{q}_t} = 0 \quad (20)$$

where $q_t(t)$ is the degrees of freedom at the joints and bogies of vehicles. Thus, the equations of motion can be expressed by the degrees of freedom of joints, bogies, and a bridge.

The vertical interactive force between the first axle of j -th bogie and the rail is expressed as in Eq. (21).

$$F_b^{j1} = (M_s^{j1} + m_u)g + c_p \dot{v}_r^{j1} + k_p v_r^{j1} - m_u(\ddot{v}_b^{j1} + l_0 \cos \phi_0 \ddot{\phi}_b^{j1}) \quad (21)$$

where M_s^{j1} and m_u are respectively the sprung mass and unsprung mass (wheel and axle) of primary suspension and g is gravity acceleration.

In modeling the bridge with beam elements, the vertical interactive force as in Eq. (21) is transferred to the node by interpolation. Then the equation of motion of the bridge is given as

$$[M_b]\{\ddot{q}_b(t)\} + [C_b]\{\dot{q}_b(t)\} + [K_b]\{q_b(t)\} = \{P_b(t)\} \quad (22)$$

where $[M_b]$, $[C_b]$, $[K_b]$, and $\{q_b(t)\}$ are the mass matrix, stiffness matrix, damping matrix, and vector of nodal degrees of freedom of the bridge, respectively and $\{P_b(t)\}$ is the load vector transferred to the node.

From the above Eqs. (20), (21), and (22), the equation of motion of the total vehicle-bridge system is derived as given in Eq. (23).

$$[M_{total}(t)]\{\ddot{q}(t)\} + [C_{total}(t)]\{\dot{q}(t)\} + [K_{total}(t)]\{q(t)\} = \{P_{total}(t)\} \quad (23)$$

where $[M_{total}(t)]$, $[C_{total}(t)]$, and $[K_{total}(t)]$ are respectively the mass matrix, damping matrix, and stiffness matrix of total vehicle-bridge system which vary with time as these matrices are determined by the positions of vehicles. $\{P_{total}(t)\}$ is the load vector and $\{q(t)\} = \langle q_b(t) \quad q_t(t) \rangle^T$ is the vector composed of nodal degrees of freedom of the bridge and degrees of freedom of car bodies and bogies. $[M_{total}(t)]$ is composed of mass matrices of the bridge ($[M_b]$), unsprung mass of train ($[M_u(t)]$), the front power car ($[M_f(t)]$), passenger cars ($[M_{tp}(t)]$), and the rear power car ($[M_{tr}(t)]$). $[C_{total}(t)]$ is composed of damping matrices of the bridge ($[C_b]$) and the train ($[C_t(t)]$). $[K_{total}(t)]$ is composed of stiffness matrices of the bridge ($[K_b]$) and the train ($[K_t(t)]$). And, $[P_{total}(t)]$ is the load vector of the bridge ($[P_b(t)]$) and the train ($[P_t(t)]$). To obtain the numerical solution for the equation of motion of total vehicle-bridge system, Newmark's β method with average acceleration ($\gamma = 1/2$ and $\beta = 1/4$), which is unconditionally stable, is used.

5. Numerical examples

5.1 Numerical verifications

The model presented in this study is verified by comparing the analysis results with the experimental results. The experimental results were obtained by operating 20-car formation high-speed train on 2-span continuous PC box girder railway bridge (Kim *et al.* 2001 and Choi 2001). 20-car formation high-speed train is composed of 2 power cars, 2 power passenger cars, and 16 passenger cars, which are operated on the railway bridge at the speed of 300 km/h in this verification. 2-span continuous PC box girder railway bridge is the 14 m-width bridge with ballasted double tracks, which have the eccentricity of 2.5 m.

The vertical deflections at the center of the bottom slab were adopted as the measured data in the *in situ* test. The experimental results of this verification were obtained by low pass digital filtering for the frequency over 10 Hz of the measured data. Because the natural frequency for the main modes of the vehicles and bridge were surely proved to be below 10 Hz through the spectral analysis of the measured data. The vertical deflections were measured at the mid-points A and B of each span as shown in Fig. 8(a). Total 76 beam elements are used to model the bridge, which have 8 types of cross sections to model the various cross section.

In Fig. 8(b) and (c), the analysis results are compared with the experimental results after filtering. Because there can be errors in the calibration of the *in situ* test, construction of the bridge, calculation of the cross-sectional properties, and evaluation of mass and damping ratio, there exist a

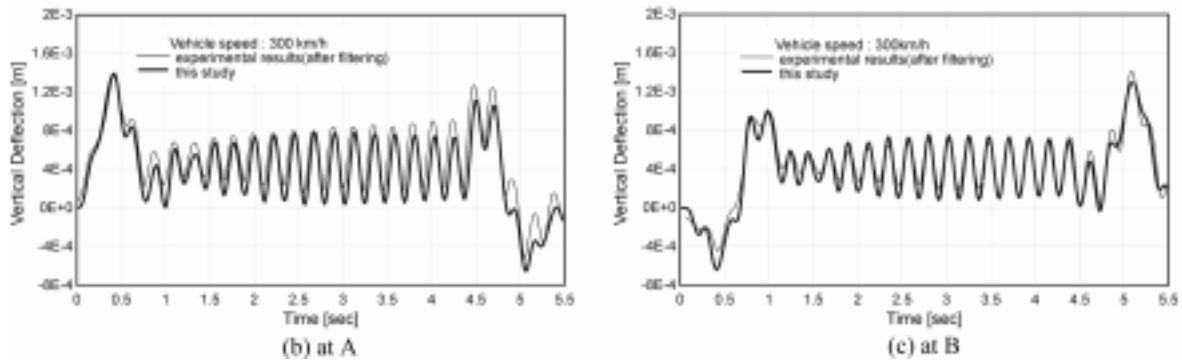
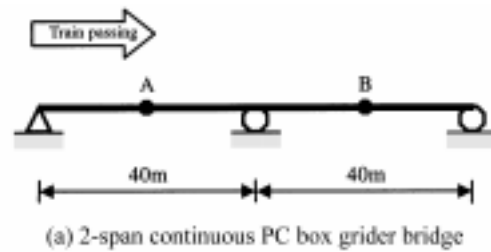


Fig. 8 Comparison of the analysis results with the experimental results

Table 1 The details of the bridge

Bridge type		3-span continuous PC box girder bridge
Details	Span length	3@25 m = 75 m
	Breadth	14 m
	Height	3.5 m
	Track	Distance between double tracks = 5 m
Live loads		Axle loads (2 power cars, 15 passenger cars)
Material properties	Young's modulus	$3.6 \times 10^5 \text{ kg/cm}^2$
	Damping ratio	5%
	Mass density	4,812 kg/m^3
	Poisson's ratio	0.2

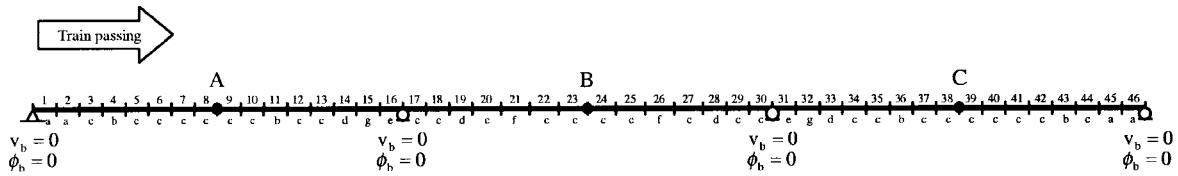


Fig. 9 Modeling of 3-span continuous PC box girder bridge with beam elements

Table 2 Modeling of the bridge with beam elements

(a) the lengths of elements

Lengths of elements (m)	Element ID No.
1.000	4, 11, 21, 26, 36, 43
1.500	2, 5, 6, 7, 8, 9, 10, 37, 38, 39, 40, 41, 42, 45
1.525	12, 13, 34, 35
1.550	20, 27
1.600	14, 15, 18, 19, 28, 29, 32, 33
1.700	1, 46
2.250	16, 17, 22, 23, 24, 25, 30, 31
2.300	3, 44

(b) the properties of types of cross sections

Types of cross sections	Area (m^2)	Moment of inertia (m^4)	Torsional constant (m^4)
a	14.832	12.215	172.028
b	11.278	12.793	135.699
c	10.046	10.061	131.168
d	10.882	12.737	134.959
e	12.313	11.568	159.633
f	11.053	12.827	135.738
g	13.498	13.464	162.963

little discrepancies between the analysis results and the experimental results. In spite of many uncertainties and the simplification of the bridge and vehicle models in this study, the vertical deflections of the analysis results are well agreed with the experimental results.

Table 3 Dynamic properties of the vehicle in analysis

ITEM	Motor coach motor bogie	Trailer motor bogie	Intermediate carrying bogie
Train speed	200 km/h~400 km/h		
Car body mass (kg)	51,152	38,770	22,560
Bogie mass (kg) (including unsprung mass)	7,057	7,057	7,057
Unsprung mass (kg)	4,096	4,096	4,096
Load/axle (kg _f)	17,000	17,000	17,000
Inertia moment of car body (gallop motion, kg · m ²)	1,054,325	804,420	599,264
Inertia moment of bogie (gallop motion, kg · m ²)	1,487	1,487	1,487
Primary suspension - vertical spring(kg _f /m)	510,200 (=255,100/axle)	510,200 (=255,100/axle)	291,500 (=145,800/axle)
Secondary suspension - vertical spring(kg _f /m)	255,100	85,030	60,020
Primary suspension Damper - vertical (kg _f · sec/m)	4,082 (=2,041/axle)	4,082 (=2,041/axle)	4,082 (=2,041/axle)
Secondary suspension Damper - vertical (kg _f · sec/m)	2,041	2,041	1,020

5.2 Analysis of an existing bridge

5.2.1 The bridge under consideration

The vehicle-bridge interaction analysis scheme suggested in this study is used to analyze a 3-span continuous straight PC box girder railway bridge. The details of the bridge for analysis are given in Table 1. Since the cross section of the bridge varies in the length direction, it is modeled by beam elements of segment-wise constant sections (Fig. 9). Total 46 beam elements of 7 different cross sections are used in modeling the entire bridge. Details are given in Table 2(a) and Fig. 9, in which ID numbers of the beam elements used to model the bridge are given. The values of area, moment of inertia of area, and torsional constant of 7 different types of cross sections are listed in Table 2(b).

5.2.2 Vehicle details

Dynamic properties of the vehicle used in this analysis are given in Table 3. Bogies are classified into three categories; motor coach motor bogies, trailer motor bogies, and intermediate carrying bogies.

5.2.3 The influence of the eccentricity of axle loads

To investigate the influence of the eccentricity of axle loads, the results from this study are compared with those of the analysis for moving constant force and those of 2-dimensional vehicle-

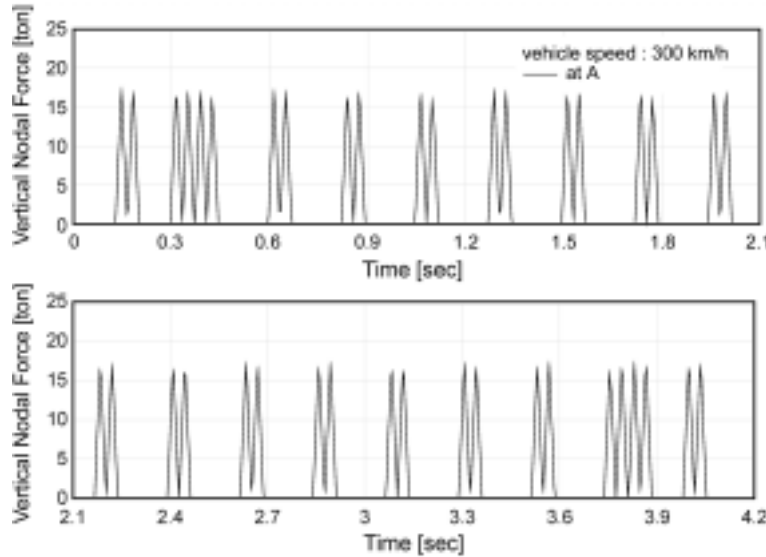


Fig. 10 Vertical nodal force at point A generated by axle loads

bridge interaction analysis not considering the eccentricity. In the analysis for moving constant force, it is assumed that there are no inertia effect and damping effect resulting from the mass and damping mechanism of a bridge. As the train passes through the bridge from the left to the right, the vertical deflections and torsional rotations in the centroids of cross sections at the mid-points of each span, i.e., points A, B, and C in Fig. 9, are obtained. In the case that double tracks are constructed on the bridge, the main loads acting on the bridge are the vertical and torsional forces transmitted through vehicle axles. Nodal force vector is constructed by the weights of vehicles and the elevation of track irregularities according to the positions of vehicles as time goes by. For example, the vertical nodal force acting on point A as the vehicle moves is shown in Fig. 10.

The vertical deflections at points A, B, and C are shown in Fig. 11 when vehicle moves along track with a speed of 300 km/h. Two outstanding vertical deflections at each of points A, B, and C are produced at the time when two bogies set up between a power car and a passenger car pass through these points. Because the structure of the bridge is symmetric about the mid-length point of the bridge and a series of axle loads are also nearly symmetric as shown in Fig. 10, the maximum value of vertical deflections at points A and C are almost the same. However, the amplitude of vertical deflection at A is larger than those at other two points not only when bogies of passenger cars pass by but also after the vehicle passes through the bridge completely. Therefore, it is observed that the first span (point A), which the vehicle arrives first, is more affected by the dynamic effect of vehicle movement than any other spans. As shown in Fig. 12, torsional rotations show the tendency similar to vertical deflections, that the peak magnitude descends sequentially in the order of C, B, and A and torsional rotations have the components of higher frequencies of vibration at B than A and C. Torsional rotations at A, B, and C have nearly the same maximum values. The maximum discrepancy between torsional rotations from this study and those of the analysis for moving constant force is most clearly seen at B. And the time histories of torsional rotations at A and C show the same fashion if one of these are reversed.

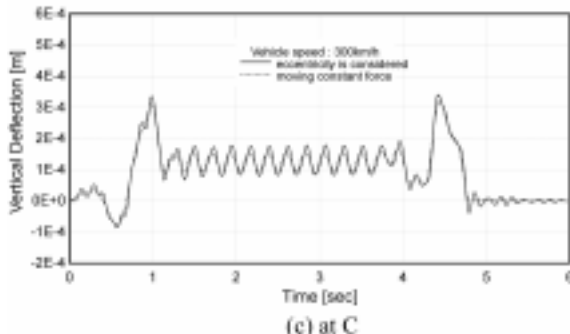
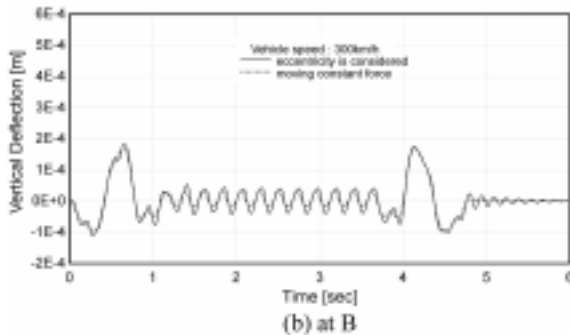
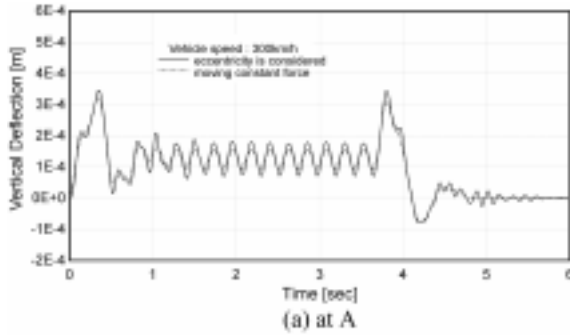


Fig. 11 Vertical deflections in considering the eccentricity of axle loads and in moving constant force analysis

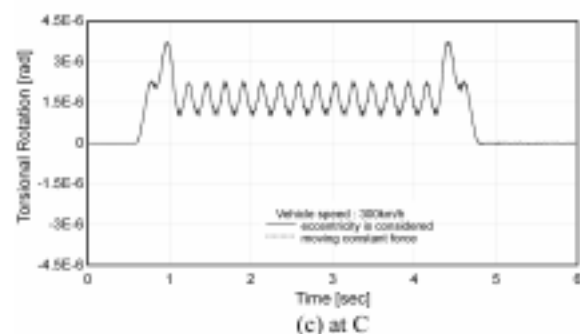
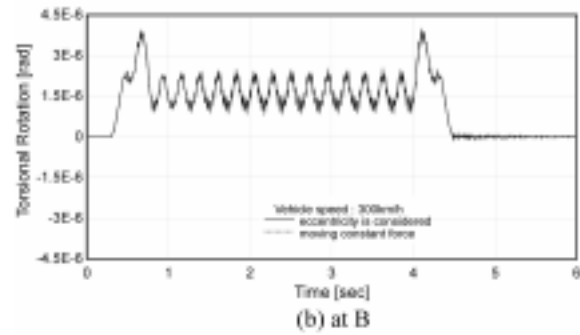
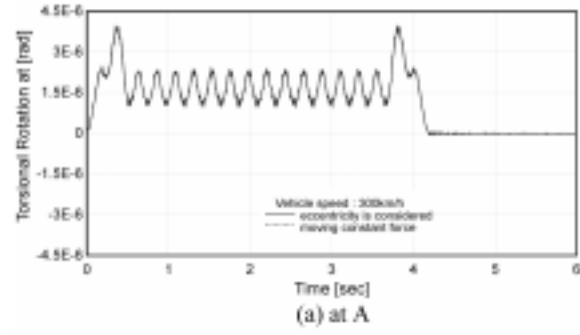


Fig. 12 Torsional rotations in considering the eccentricity of axle loads and in moving constant force analysis

In Fig. 13, the vertical deflections at points A, B, and C are compared to the cases with and without the eccentricity of 2.5 m of vehicle axle loads. The difference in vertical deflections caused by the eccentricity is not significant except at $t = 0.4$ sec when two bogies set up between a front power car and a passenger car pass through the point A for the first time. At this time, relatively large deflections are observed at point A, and the vibration with high frequencies appear due to the effect of torsional vibrations (Fig. 12).

The spectral densities of vertical deflections at the mid-points of spans, which are generated by fast Fourier transform (FFT), are shown in Fig. 14. When a series of vehicle axle loads are acted on the bridge, the heavy spectral densities at zero frequency of points A and C are observed while a quite different pattern of spectral density of vertical deflection at B is shown reflecting the vertical

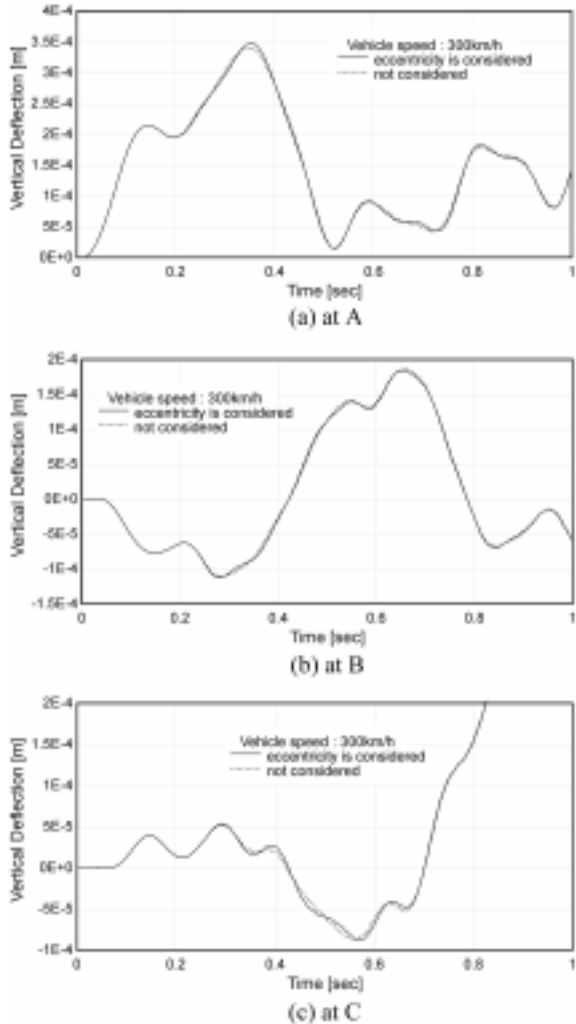


Fig. 13 Vertical deflections in considering the eccentricity of axle loads and not

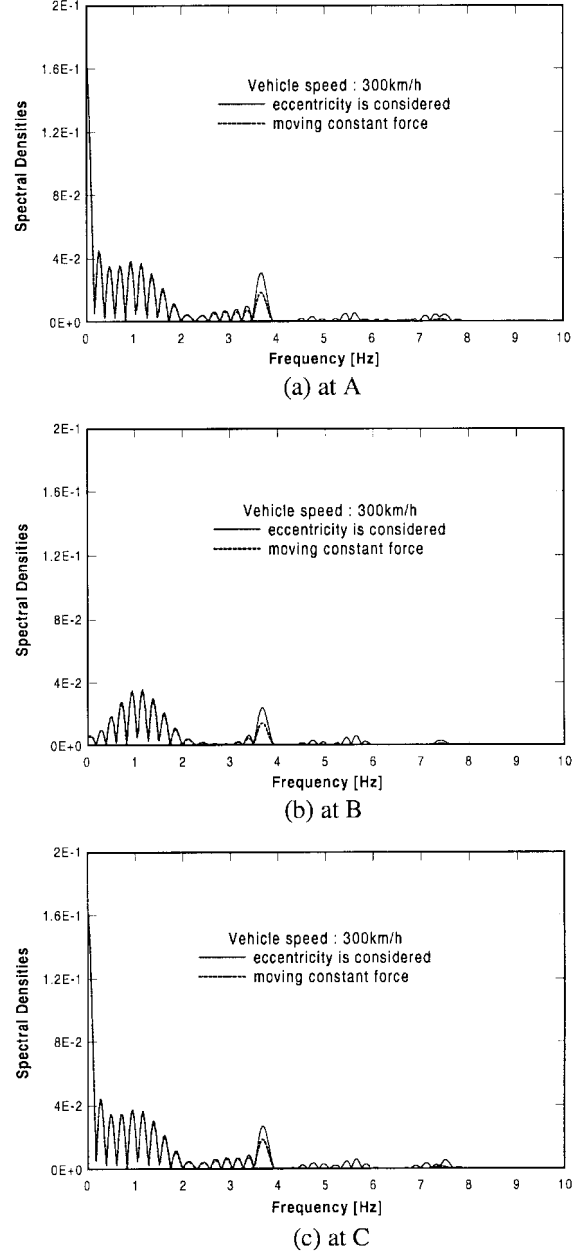
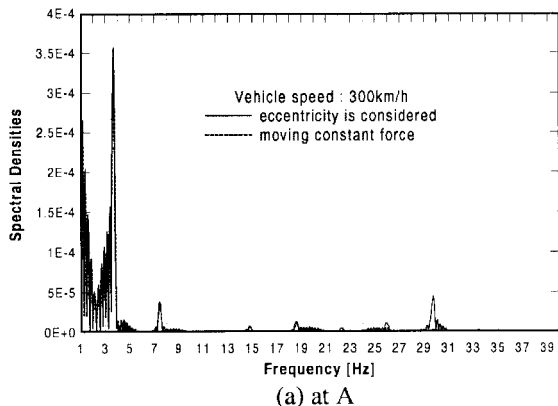
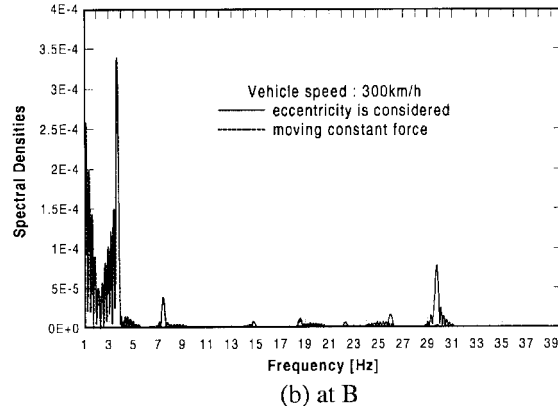


Fig. 14 Spectral densities of vertical deflections in considering the eccentricity of axle loads and in moving constant force analysis

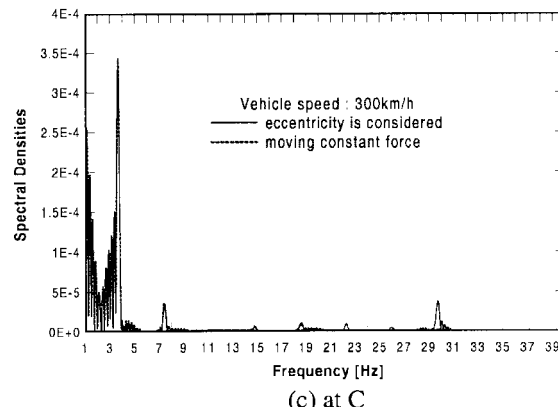
deflection at B which vibrates up and down the neutral axis. The heavy spectral densities of vertical deflections at A, B, and C are observed at 1 Hz and 3.7 Hz. The heavy spectral density of 1 Hz is induced by axle loads of bogies set up between power cars and passenger cars and that of 3.7 Hz is



(a) at A

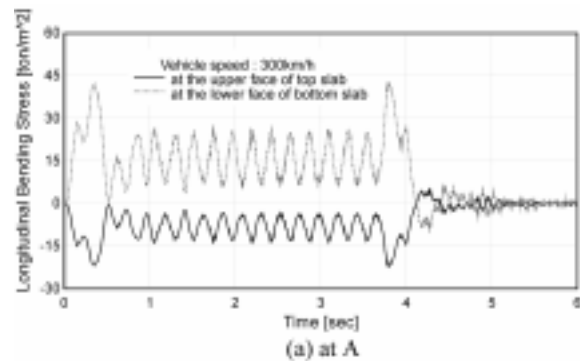


(b) at B

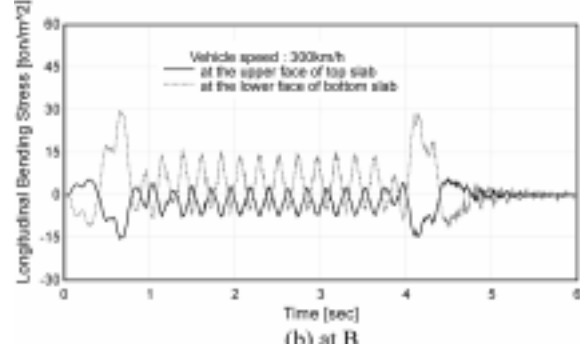


(c) at C

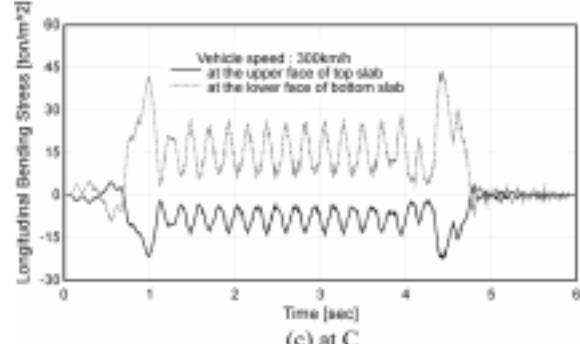
Fig. 15 Spectral densities of torsional rotations in considering the eccentricity of axle loads and in moving constant force analysis



(a) at A



(b) at B



(c) at C

Fig. 16 Longitudinal bending stress when one train moves

induced by the axle loads of bogies set up in passenger cars. The distributions of the spectral densities for vertical deflections at A, B, and C are almost identical to those of the analysis for

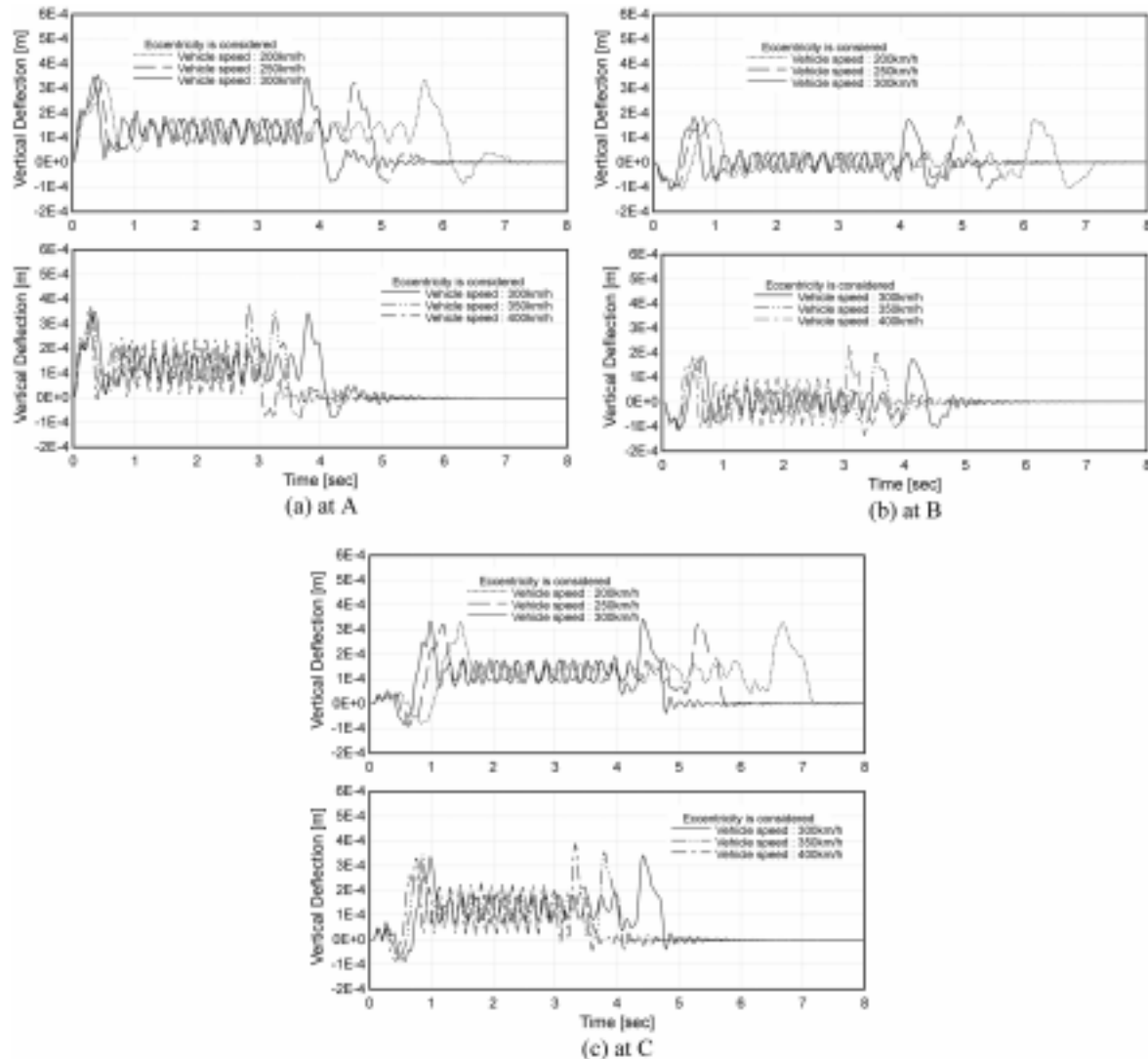


Fig. 17 Vertical deflections as the increase of vehicle speed

moving constant force in the range less than 3 Hz and a denser distribution than the analysis for moving constant force is observed in the high frequency range between 3 Hz and 8 Hz. Such a phenomenon is due to the vibrations with high frequencies included by the actions of torsional forces, torsional rotations and vehicle-bridge interactions.

The spectral densities of torsional rotations in the mid-points of spans, which are generated by FFT, are shown in Fig. 15. It is observed that the spectral densities of torsional vibrations with higher frequencies than vertical deflections appear and the spectral densities of 30 Hz is remarkable in particular. All the spectral densities of torsional rotations at A, B, and C are similar except the spectral densities of 30 Hz at B which is more significant than at A and C.

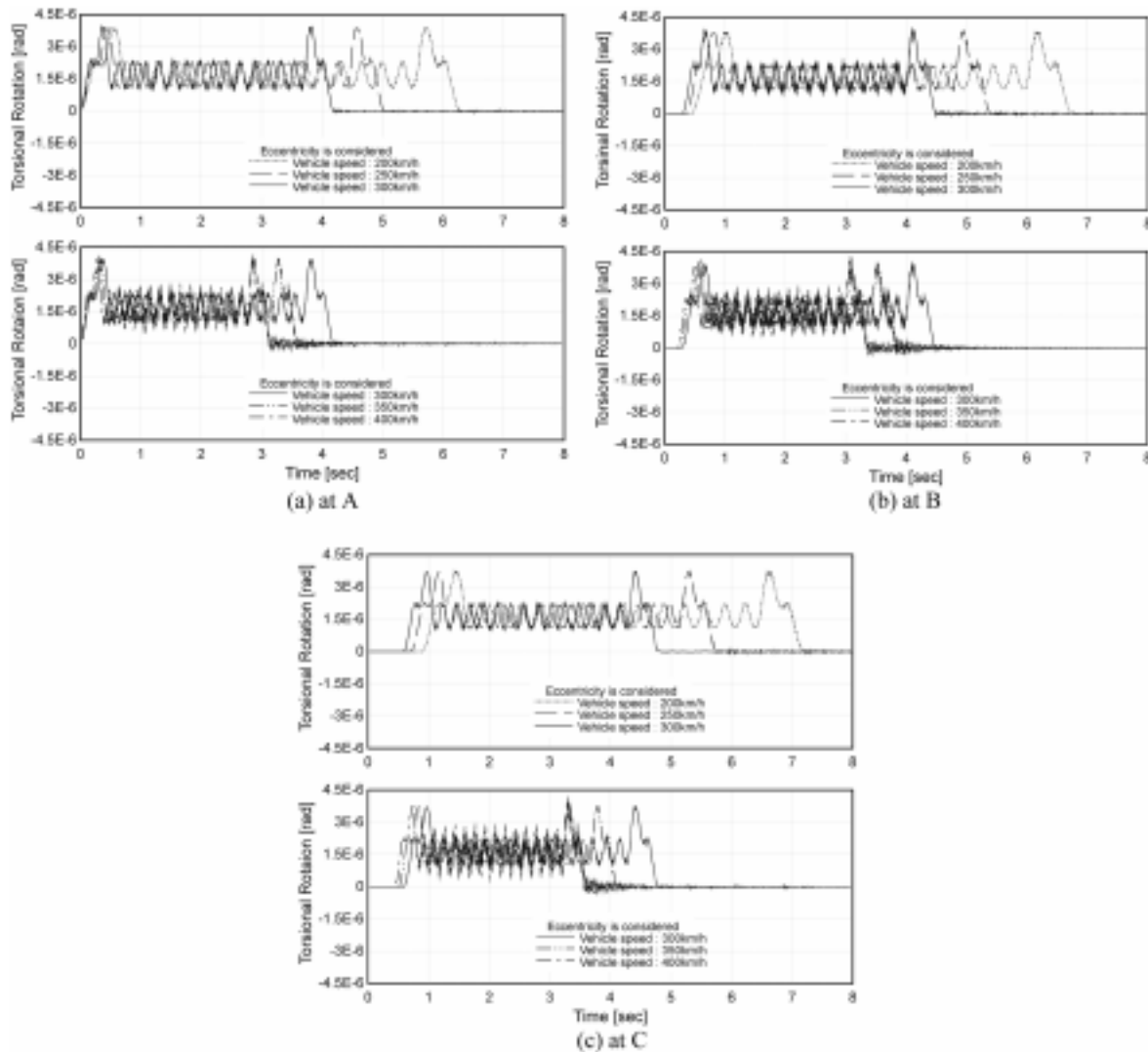


Fig. 18 Torsional rotations as the increase of vehicle speed

Once nodal displacements have been calculated from the analysis, member forces for the structural behavior can be calculated. The main member force in a bridge is the longitudinal bending stress generated by bending moments. Longitudinal bending stress can be calculated from flexure formula, in which bending moments can be evaluated by multiplying the element stiffness matrix by the nodal displacements in local coordinate system. The longitudinal bending stresses at points A, B, and C at the upper face of top slab and at the lower face of bottom slab when one train moves, are shown in Fig. 16. Compressive stress is indicated to be negative and tensile stress is to be positive. In addition, the stresses calculated in the above-mentioned stress analysis can be used to determine the fatigue lives of structural members.

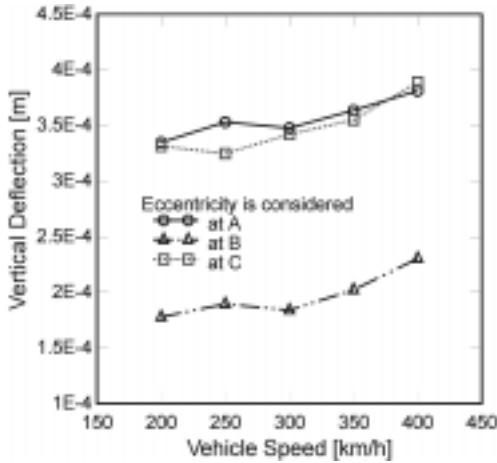


Fig. 19 The change of vertical deflections as the increase of vehicle speed

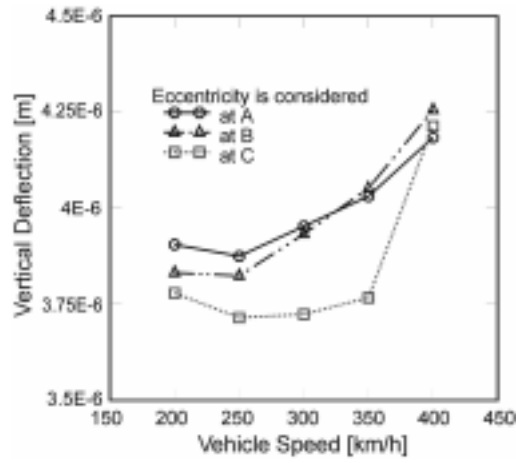


Fig. 20 The change of torsional rotations as the increase of vehicle speed

5.2.4 The Influence of the vehicle speed

Once the bridge has been constructed and the running vehicle has been determined, the vehicle speed is the only variable parameter left undecided. Therefore, it should be of interest to investigate the dynamic behavior of the bridge with different vehicle speeds.

In cases that vehicle speeds are respectively 200 km/h, 250 km/h, 300 km/h, 350 km/h, and 400 km/h, the time histories of vertical deflections and torsional rotations in the centroids of cross sections at points A, B, and C are shown in Figs. 17 and 18. As the vehicle becomes faster, the increases of vertical deflections and torsional rotations are not outstanding at the arrival of vehicle. However, when the bogies of passenger cars pass through or when the bogies set up between power cars and passenger cars pass by the mid-points of spans, the increases become more significant.

As the vehicle becomes faster, the change of the maximum vertical deflections is shown in Fig. 19.

Table 4 Comparison of the maximum deflections with allowable values for serviceability

Specifications	Vertical deflections	Torsional rotations
UIC code	$\Delta_{\max}/L \leq 1/1700$	0.4 mm per 3 m in longitude and 1 m in transverse
	5.882×10^{-4}	0.4(mm)
Shinkansen	$v_{\max} \leq L/1800$	-
	1.389×10^{-2} (m)	-
Present study	$\Delta_{\max}/L = 1.037 \times 10^{-5}$ $v_{\max} = 3.890 \times 10^{-4}$ (m) (C, vehicle speed : 400 km/h)	7.300×10^{-5} (mm) (B, vehicle speed : 400 km/h)
	$\Delta_{\max}/L = 1.941 \times 10^{-4}$ $v_{\max} = 7.281 \times 10^{-4}$ (m) (C, vehicle speed : 400 km/h, $dx = 50$ m)	1.420×10^{-4} (mm) (B, vehicle speed : 400 km/h, $dx = 12.5$ m)

When the vehicle runs faster than 300 km/h, the maximum vertical deflection increases slowly but steadily. The change of the maximum torsional rotations, as vehicle becomes faster, is shown in Fig. 20. When the vehicle speed is in the range of 200 km/h to 300 km/h, the increases of vertical deflections and torsional rotations are not so significant, on the other hand, when the vehicle speed is higher than 300 km/h, the increases of vertical deflections and torsional rotations become a little more significant. The fundamental frequency of the analyzed bridge is 6.8 Hz and the effective beating interval for the present type of the vehicle is 18.7 m. Therefore, the critical velocity, which is originated from the concept of the resonance under the passage of uniformly distributed load, is 457.78 km/h. The critical velocity is sufficiently deviated from the highest speed of the present type of vehicle, i.e., 350 km/h.

Bridges on which a high-speed vehicle moves are to be designed to insure the structural safety and the comfort of passengers. To satisfy these requirements, the allowable deflections are specified in several design codes such as the International Railway Federation (UIC) and the specifications of designing bridges for Shinkansen. The maximum vertical deflections and torsional rotations evaluated by the method proposed in this study are compared with the allowable values by the codes/specifications and shown in Table 4. Even though the high-speed vehicle moves on the bridge of current analysis with a speed of 400 km/h which is much higher than commercial operation speed, the maximum vertical deflections and torsional rotations are much less than the allowable values presented in the UIC code and the specifications of Shinkansen.

5.2.5 The Influence of the speed of two vehicles on double tracks

Investigations into the influence of vehicle speed on vehicle-bridge interactions are also carried out for the case that two trains move respectively on their tracks in the opposite direction. It is assumed that the train enters into the bridge first from the left as shown in Fig. 21 and that two trains move at the same speed. The train speeds considered are 200 km/h, 250 km/h, 300 km/h, 350 km/h, and 400 km/h. Because the arrival time of two trains are different, after the first train has passed some distance on the bridge, the other train enters into the bridge from the opposite direction. Seven different cases of passed distances (dx) of the first train before the other train enters into the bridge are considered, i.e., 0 m, 12.5 m, 25 m, 37.5 m, 50 m, 62.5 m, and 75 m. For the five different cases of vehicle speeds, the changes of vertical deflections and torsional rotations at A, B, and C are examined with different dx .

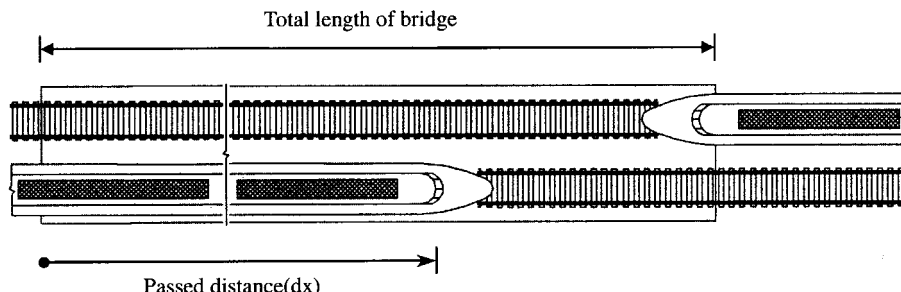


Fig. 21 Passed distance (dx) of the first train until the other enters into the bridge

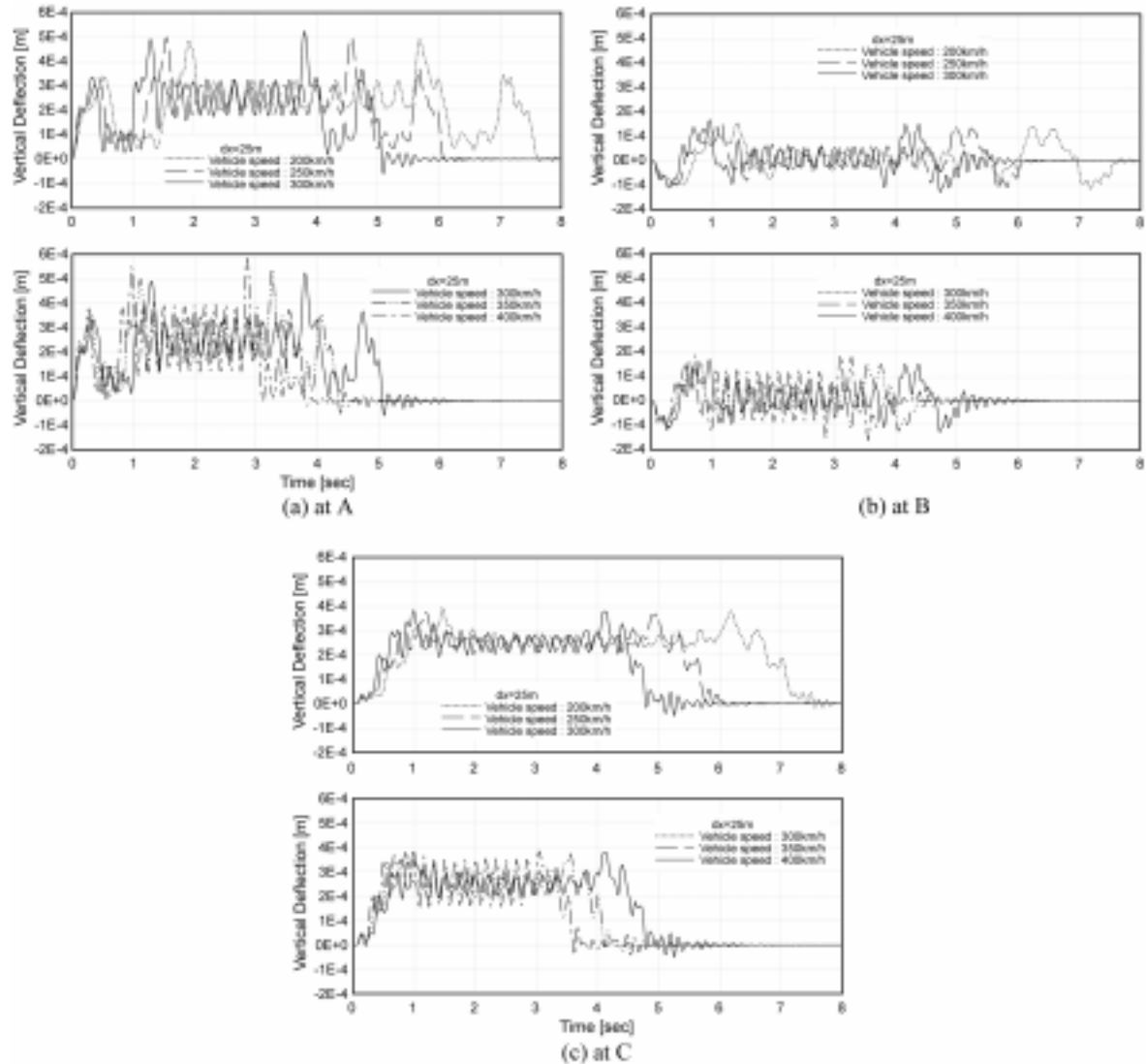


Fig. 22 Vertical deflections as the increases of the speeds of two trains ($dx = 25$ m)

As the vehicle becomes faster, the vertical deflections and torsional rotations in the centroids of cross sections at the mid-points of spans due to two trains on double tracks are shown in Figs. 22 and 23 for the typical case that the passed distance (dx) of the first train is 25 m. In this case, it takes 0.45, 0.36, 0.3, 0.26, and 0.23 seconds for the first train to move 25 m with the five different vehicle speeds, respectively. After these time periods, the other train enters into the bridge and the dynamic responses of bridges induced by two moving trains are observed. The dynamic responses of bridges are more complicated than those for a single moving train as shown in Figs. 11 and 12. It is observed that the time histories of vertical deflections and torsional rotations include the higher frequency components when two trains move on the bridge than when a single train moves.

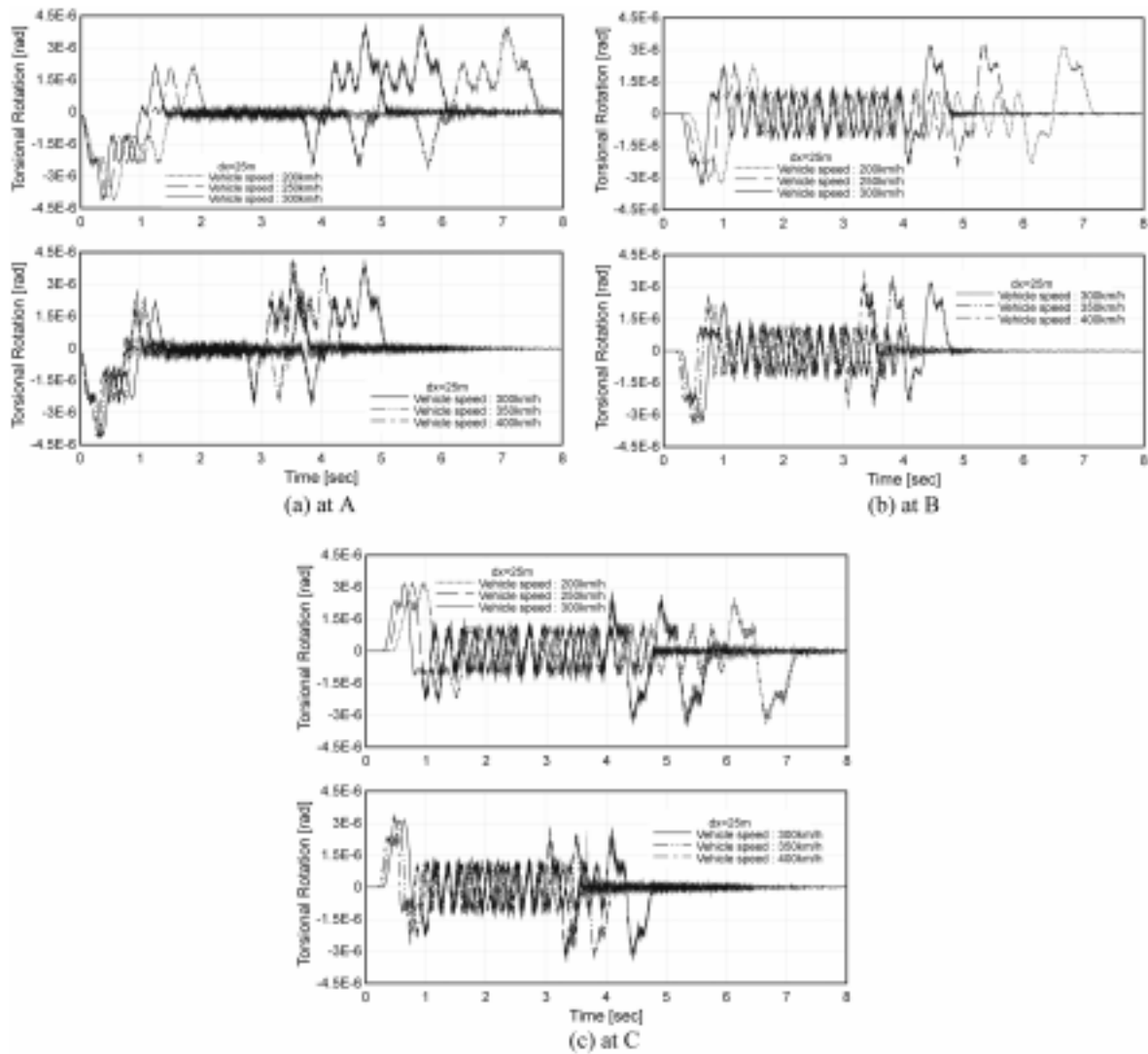


Fig. 23 Torsional rotations as the increases of the speeds of two trains ($dx = 25$ m)

In Table 5, the values of dx that generate the maximum vertical deflections and torsional rotations at points A, B, and C are listed for the speeds of two trains. From the analysis results at A, B, and C, the following facts are observed. When the first train passes the mid-point of the third span from the left of the bridge and the other train enters into the bridge, the maximum vertical deflections are generated at A. And, when the first train passes the center span of the bridge and the other train enters into the bridge, the maximum torsional rotations are generated at A. When two trains enter into the bridge simultaneously, the maximum vertical deflections are generated at B. When the first train passes the mid-point of the center span of the bridge and the other train enters into the bridge, the maximum torsional rotations are generated at B. When the first train passes the third support from the left of the bridge and the other train enters into the bridge, the maximum vertical

Table 5 Passed distances (dx , m) generating the maximum vertical deflections for the speeds of two trains

Response	for max. vertical deflection			for max. torsional rotation			
	Position	A	B	C	A	B	C
Vehicle speed (km/h)	200	62.5	12.5	62.5	12.5	37.5	25
	250	62.5	0.	50.	12.5	37.5	12.5
	300	62.5	0.	50.	37.5	37.5	0.
	350	62.5	0.	50.	50.	37.5	12.5
	400	62.5	0.	50.	37.5	75.	12.5

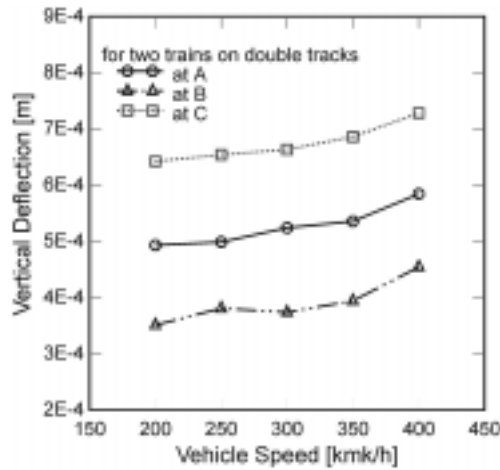


Fig. 24 The change of vertical deflections as the increases of the speeds of two trains

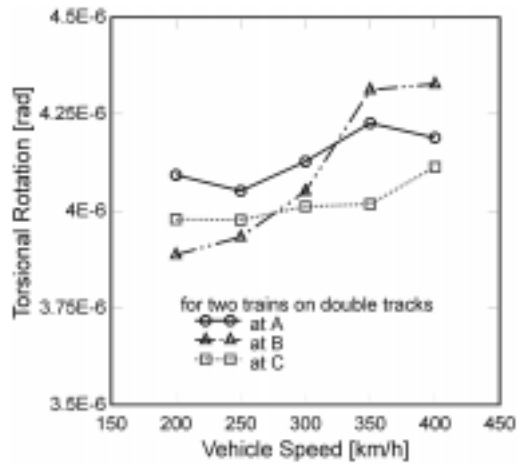


Fig. 25 The change of torsional rotations as the increases of the speeds of two trains

deflections are generated at C. And when two trains enter into the bridge simultaneously, the maximum torsional rotations are generated at C.

The change of the maximum vertical deflection is shown in Fig. 24 as the vehicle speed becomes higher. When the vehicle speed becomes higher than 300 km/h, the maximum vertical deflection increases steadily. It is observed that the changes of the maximum vertical deflection at A and B have similar tendencies. The change of the maximum torsional rotation is shown in Fig. 25 as vehicle speed becomes higher. The maximum torsional rotations at A, B, and C are increased somewhat irregularly as vehicle speed increases, however, in case that the vehicle speed reaches 400 km/h the maximum torsional rotations at B are increased significantly. As shown in Table 4, although the two trains move on double tracks of the bridge with the speed of 400 km/h in the opposite direction, the maximum vertical deflections and torsional rotations are less than the allowable values presented in the UIC code and the specifications of Shinkansen.

The vertical deflections and torsional rotations are shown in Figs. 26 and 27 when one or two trains move on the bridge. In case of two trains, when the passed distance (dx) of the first train is 25 m, or 0.3 seconds after the entering of the first train, the other train enters into the bridge and the

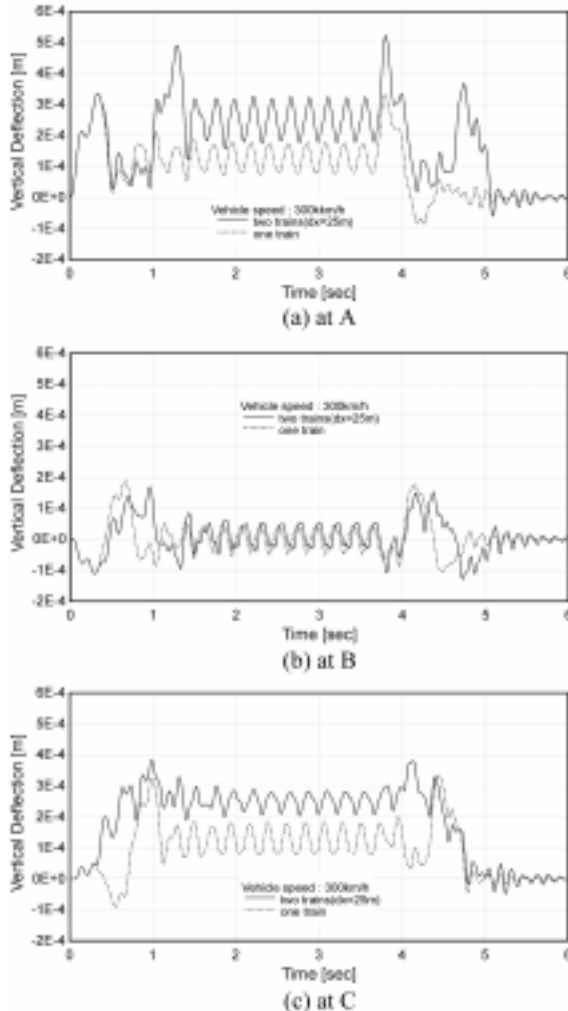


Fig. 26 Vertical deflections when one train moves and when two trains move

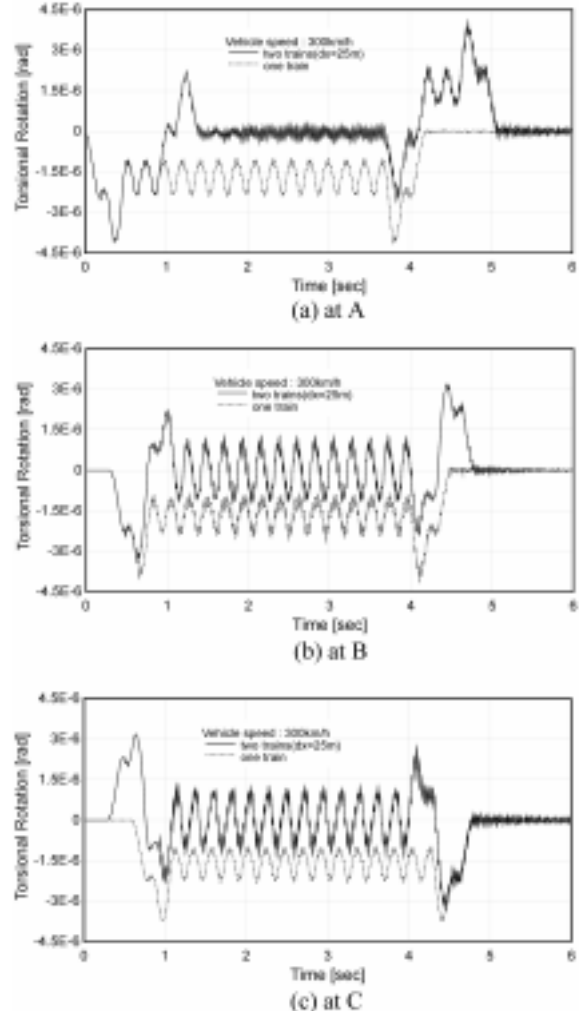


Fig. 27 Torsional rotations when one train moves and when two trains move

influence of the second moving train is shown. By investigating the ratio of the maximum responses for the case of two trains to those for the case of one train, the influence of two trains moving on the bridge can be indirectly compared with that of one train. As the speeds of two trains become higher, the ratio of the maximum vertical deflections for the case of two trains to those for the case of one train is shown in Fig. 28. The ratios at B and C are decreased while it is increased at A. The ratio of the maximum torsional rotations for the case of two trains to those for the case of one train is shown in Fig. 29. As the speeds of two trains become higher, the ratios at A and C are decreased while increased at B. The vertical deflections at each span when two trains move are larger than those when one train moves but the torsional rotations at C when two train move become smaller than those when one train moves as the speeds of two trains become higher.

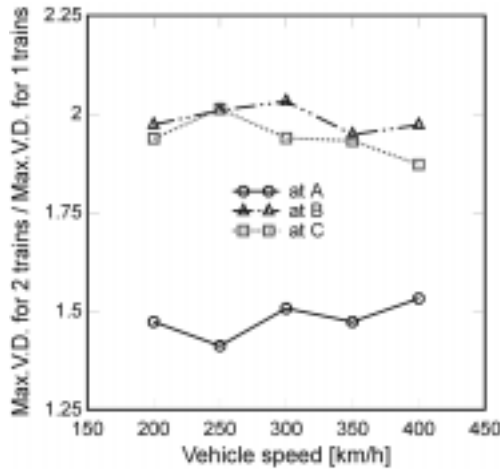


Fig. 28 The ratio of the maximum vertical deflections for two trains to those for one train

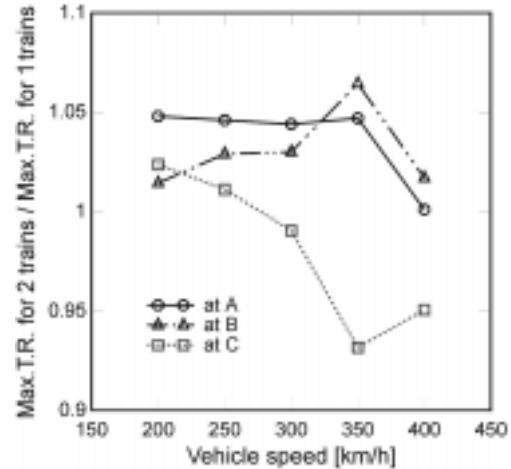


Fig. 29 The ratio of the maximum torsional rotations for two trains to those for one train

6. Conclusions

In this study, the analysis of high-speed vehicle-bridge interactions by a simplified 3-dimensional finite element model was performed. By using this model, which includes the eccentricity of axle loads and the effect of the torsional forces acting on the bridge, the more efficient and accurate vehicle-bridge interaction could be obtained. For the verification of this model, the analysis results were compared with the experimental results and were well agreed with the experimental results. Also, the investigation into the influences of the eccentricity of vehicle axle loads and the vehicle speed on vehicle-bridge interaction were carried out. Finally, the calculation of the longitudinal bending stress was performed. In the future study, the additional fatigue analysis based on the stress analysis should be carried out to evaluate the fatigue life of railway bridges.

The difference of the vertical deflections in the centroids of cross sections of the bridge caused by the eccentricity of vehicle axle loads was not significant except when two bogies set up between the front power car and the passenger car passed through the mid-point of the first span for the first time. The difference, however, can be more seriously amplified in the cases of torsionally flexible bridges. And in that case, the consideration of the eccentricity of vehicle axle loads is essential to obtain the accurate behavior of a bridge. By considering the eccentricity of axle loads, the components of high frequencies could be included in vertical deflections and torsional rotations.

It is of special interest to see the influence of the train speed exceeding current practiced limit of 300 km/h. The influence of the vehicle speed on the maximum responses of the bridge is not significant within the maximum operational speed limit of 300 km/h. However, when the train speed exceeds 300 km/h, the influence becomes more significant. For example, for a single train passing, the magnitude of the maximum vertical deflection at the mid-point of the middle span increased by 25% as the change of the train speed from 300 km/h to 400 km/h. And the magnitude of the

maximum torsional rotation at the mid-point of the last span increased by 13% as the change of the train speed from 300 km/h to 400 km/h. The critical velocity was 457.78 km/h, which was sufficiently deviated from the highest speed of the present type of vehicle, i.e., 350 km/h.

The maximum vertical deflections and torsional rotations in the analysis results of numerical examples were much less than allowable values described in major design codes, including the UIC code and the specifications of Shinkansen, to secure the serviceability and safety of the bridge.

References

- Bathe, K.J. (1996), *Finite Element Procedures*, Prentice-Hall, USA.
- Bhatti, M.H. (1982), "Vertical and lateral dynamic response of railway bridges due to nonlinear vehicles and track irregularities", Ph.D. Thesis, Illinois Institute of Technology, Chicago, USA.
- Chang, T.P. and Liu, Y.N. (1996), "Dynamic finite element analysis of a nonlinear beam subjected to a moving load", *Int. J. Solids and Struct.*, **33**(12), 1673-1688.
- Choi, C.K., Song, M.K. and Yang, S.C. (1999), "Simplified 3-dimensional high-speed vehicle-bridge interaction analysis considering the eccentricity of vehicle axle loads", *Proc. of the First Int. Conf. on Advances in Struct. Eng. and Mech.*, **2**, 1601-1608.
- Choi, C.K., Song, M.K. and Yang, S.C. (2000), "Influence of vehicle speed on high-speed vehicle(TGV)-bridge interactions", *J. Korean Society of Civil Engineers*, **20**(1-A), 27-38.
- Choi, S.L. (2001), "Modeling methods of high-speed railway train for dynamic response analysis of railway bridges", M.S.D. Thesis, Yonsei University, Korea.
- Chopra, A.K. (1995), *Dynamics of Structures*, Prentice-Hall, USA.
- Clough, R.W. and Penzien, J. (1993), *Dynamics of Structures*, McGraw-Hill.
- Chu, K.H. and Garg, V.K. (1979), "Railway-bridge impact: simplified train and bridge model", *J. Struct. Div., ASCE*, **105**(ST9), 1823-1845.
- Chu, K.H., Garg, V.K. and Wang, T.L. (1986), "Impact in railway pre-stressed concrete bridges", *J. Struct. Eng., ASCE*, **112**(5), 1036-1051.
- Delgado, R.L. and dos Santos R.C., S.M. (1997), "Modeling of railway bridge-vehicle interaction on high speed tracks", *Comput. & Struct.*, **63**(3), 511-523.
- Fafard, M., Bennur, M. and Savard, M. (1996), "A general multi-axle vehicle model to study the bridge-vehicle interaction", *Eng. Computations*, **14**(5), 491-508.
- Fryba, L. (1972), *Vibration of Solids and Structures under Moving Loads*, Noordhoff International Publishing, The Netherlands.
- Fryba, L. (1996), *Dynamics of Railway Bridges*, Thomas Telford House, Czech Republic.
- Garg, V.K. and Dukkipati, R.V. (1984), *Dynamics of Railway Vehicle Systems*, Academic Press, Canada.
- Hino, J., Yoshimura, T. and Konishi, K. (1984), "A finite element method prediction of the vibration of a bridge subjected to a moving vehicle load", *J. Sound and Vib.*, **96**(1), 45-53.
- Inbanathan, M.J. and Wieland, M. (1986), "Bridge vibrations due to vehicle moving over rough surface", *J. Struct. Eng., ASCE*, **113**(9), 1994-2008.
- Kim, S.H., Kim, B.S., Huh, J.Y. and Choi, S.L. (2001), "Verified 2-car model of high-speed train for dynamic response analysis of railway bridges", *Proc. of COSEIK Symposium-Fall 2001*, **14**(2), 485-492.
- Lin, J.Z. and Su, M.B. (1999), "The resonant vibration for a simply supported girder bridge under high-speed trains", *J. Sound and Vib.*, **224**(5), 897-915.
- Mermertas, V. (1998), "Dynamic interaction between the vehicle and simply supported curved bridge deck", *Comput. Methods Appl. Mech. Engrg.*, **162**, 125-131.
- Przemieniecki, J.S. (1968), *Theory of Matrix Structural Analysis*, McGraw-Hill, USA.
- Tanbe, M., Wakui, H. and Matumoto, N. (1997), "DIASTARS-dynamic interaction analysis for Shinkansen train and railway structure", *Proc. of WCRR'97*, Firenze, November **16-19**, 479-485.
- Tan, G.H., Brameld, G.H. and Thambiratnam, D.P. (1998), "Development of an analytical model for treating bridge-vehicle interaction", *Eng. Struct.*, **20**(1-2), 54-61.

- Wang, T.L., Garg, V.K. and Chu, K.H. (1991), "Railway bridge/vehicle interaction studies with new vehicle model", *J. Struct. Eng.*, ASCE, **117**(7), 2099-2116.
- Wiriyachi, A. (1980), "Impact and fatigue in open deck railway truss bridges", Ph.D. Thesis, Illinois Institute of Technology, Chicago, USA.
- Yang, Y.B. and Lin, B.H. (1994), "Vehicle-bridge interaction analysis by dynamic condensation method", *J. Struct. Eng.*, ASCE, **121**(11), 1636-1643.
- Yang, Y.B. and Yau, J.D. (1996), "Vehicle-bridge interaction element for dynamic analysis", *J. Struct. Eng.*, ASCE, **123**(11), 1512-1518.
- Yang, Y.B., Yau, J.D. and Hsu, L.C. (1997), "Vibration of simple beams due to trains moving at high speeds", *Eng. Struct.*, **19**(11), 936-944.
- Yang, Y.B. and Wu, Y.S. (2001), "A versatile element for analyzing vehicle-bridge interaction response", *Eng. Struct.*, **23**(5), 452-469.